JOURNAL OF SOLID STATE CHEMISTRY **122,** 394–406 (1996)
ARTICLE NO. 0133

$Bi_{26}Mo_{10}O_{\delta}$ Solid Solution Type in the Bi_2O_3–MoO_3–V_2O_5 Ternary Diagram

R. N. Vannier,[1] G. Mairesse, F. Abraham, and G. Nowogrocki

Laboratoire de Cristallochimie et Physicochimie du solide, ENSCL, BP 108, 59652 Villeneuve d'Ascq cedex, France

Received July 26, 1995; in revised form December 27, 1995; accepted January 5, 1996

$Bi_{26}Mo_{10}O_{69}$ and $Bi_{26}Mo_6V_4O_{67}$ crystallize in the monoclinic system, space group $P2/c$ with $a = 11.742(8)$ Å, $b = 5.800(7)$ Å, $c = 24.77(5)$ Å, $\beta = 102.94(6)°$, $Z = 1$ and $a = 11.633(7)$ Å, $b = 5.795(3)$ Å, $c = 24.39(2)$ Å, $\beta = 101.35(5)°$, $Z = 1$, respectively. The structures were solved from 4242 and 3614 reflections, respectively, collected on a Philips PW1100 automatic diffractometer (Mo$K\alpha$ radiation). The final R indexes are 0.048 and 0.041. The common structure consists of $[Bi_{12}O_{14}]_{\infty}$ columns along the twofold axis, connected with MoO_4 or (Mo, V)O_4 tetrahedra and isolated bismuth atoms in a quasi-planar O environment. A solid solution domain belonging to this structural type within the Bi_2O_3–MoO_3–V_2O_5 ternary diagram has been evidenced. It extends from $Bi_{25.75}Mo_{10}O_{\delta}$ to $Bi_{27.75}Mo_{10}O_{\delta}$ on the Bi_2O_3–MoO_3 line. This work was completed by a preliminary study of conduction properties.

INTRODUCTION

We recently described the BIMOVOX family of compounds, obtained by substitution for V^{V} with Mo^{VI} in $Bi_4V_2O_{11}$ according to the formulation $Bi_2V_{1-x}Mo_xO_{(11+x)/2}$ within the range $0 \leq x \leq 0.225$. For $x \leq 0.05$ the solid solution displays the $\alpha Bi_4V_2O_{11}$ structural type, and for $0.05 \leq x \leq 0.225$ a β-type structure is obtained (1). Beyond the upper limit of this solid solution, powder X-ray diffraction revealed another phase sharing apparent similar structural features with the high-temperature Bi_2MoO_6 polymorph (2).

Bi_2MoO_6, the low-temperature form, pertains to the family of bismuth molybdates which are widely used as effective catalysts for selective oxidation and ammoxidation of olefins (3, 4). However, large uncertainties remain about the Bi_2O_3–MoO_3 system, particularly in the Bi-rich part corresponding to a Bi/Mo ratio larger than 2, despite investigations performed by numerous groups (5–10).

A typical example of noncoherent results concerns the composition range Bi/Mo from 2.6 to 3.0. Erman *et al.* (6) described a phase formulated as $\sim 1.4Bi_2O_3$–MoO_3 having a solid solubility, while Miyazawa *et al.* (11) presented a new congruently melting compound with Bi/Mo = 3, formulated as $3Bi_2O_3$–$2MoO_3$ in spite of a chemical analysis yielding Bi/Mo ≅ 2.6. The existence of a solid solution extending around the $1.3Bi_2O_3$–MoO_3 composition was then confirmed by Chen and Smith (7).

More recently, the phase diagram of the Bi_2O_3–MoO_3 binary system was reinvestigated by Egashira *et al.* (8) who proposed two polymorphs for $3Bi_2O_3$–$2MoO_3$, related by a phase transition at 750°C. Last, Buttrey *et al.* (9) confirmed the $3Bi_2O_3$–$2MoO_3$ phase described as a defect fluorite structure.

In order to determine the nature of the neighboring phases around the BIMOVOX ones within the Bi_2O_3–MoO_3–V_2O_5 ternary diagram, we decided to carry out a structural approach as follows. A mixture corresponding to the formal composition, Bi_2O_3–$0.375V_2O_5$ $0.25MoO_3$, beyond the upper BIMOVOX limit $x = 0.225$, was introduced into a covered gold crucible and melted at 900°C. The melt was then slowly cooled and two types of crystals were observed: (i) red brown ones identified as β-type BIMOVOX and (ii) a small amount of yellowish others. The structure of this "yellow" phase was determined from X-ray single crystal diffraction data and the formulation $Bi_{26}Mo_6V_4O_{67}$ was deduced. We thereby believed that this phase could exhibit some structural similitude with the previously reported $Bi_{26}Mo_{10}O_{69}$ ($1.3Bi_2O_3$–MoO_3) (7, 11).

A single crystal corresponding to this composition was prepared and its structure confirmed our assumption. We concluded that a solid solution domain pertaining to this structural type was likely to exist within the Bi_2O_3–V_2O_5–MoO_3 ternary diagram and we carried out a determination of its compositional range. This work was completed by a preliminary study of conduction properties.

EXPERIMENTAL

The samples were prepared by solid state reaction in air, from stoichiometric amounts of pure oxides: Bi_2O_3

[1] To whom correspondence should be addressed.

0022-4596/96 $18.00

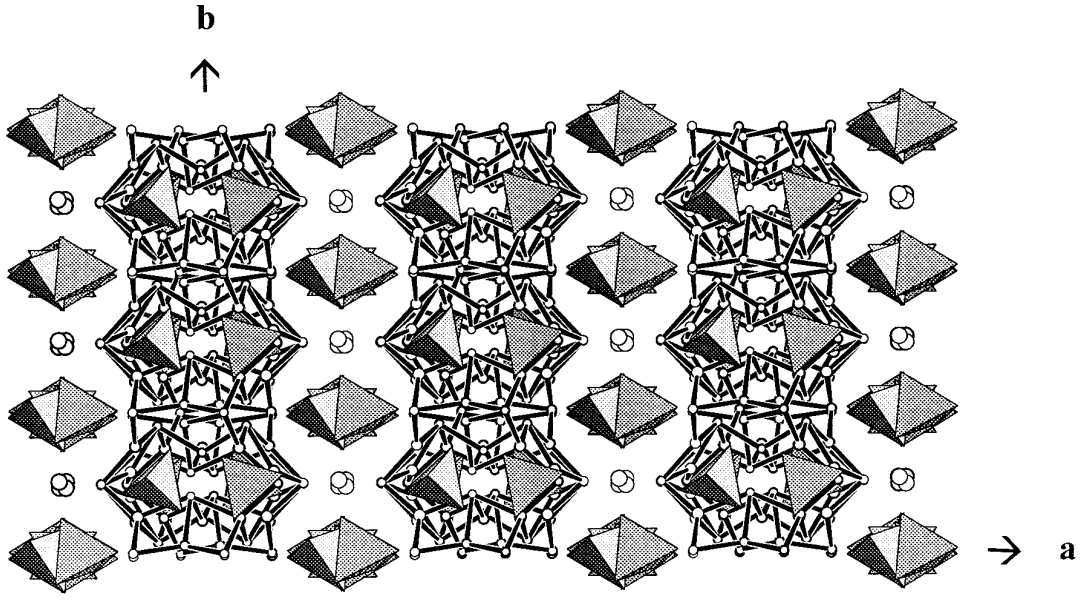

FIG. 1. (**a, b**) projection of $Bi_{26}Mo_{10}O_{\delta}$ structure with $[Bi_{12}O_{14}]_{\delta}$ columns extending along the twofold axis.

(99.9% Aldrich), previously decarbonated at 600°C, MoO_3 (Merck 99.5%), and V_2O_5 (Aldrich 99.6%). These weighed oxides, mixed and ground in an agate mortar, were first progressively preheated to 500°C in covered aluminum crucibles. They were then reground and calcinated at 800°C for 12 hr, reground, and finally treated at 850°C for 12 hr and quenched in air to room temperature. Each sample was weighed before and after each treatment; the loss was less than 0.1%.

Guinier De Wolff and Guinier Lenné focusing camera and a Siemens D5000 diffractometer (Cu$K\alpha$ radiation) were used for X-ray powder diffraction. The recording conditions on the diffractometer for most of the compounds were a 5°–60° 2θ domain, with a 0.02° step and a

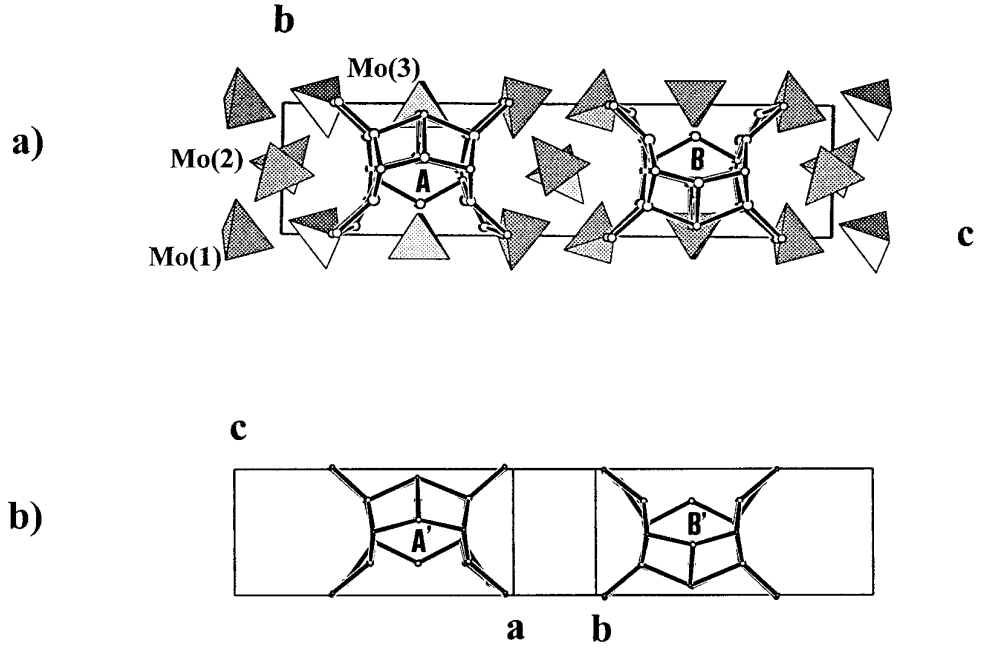

FIG. 2. (a) (**b, c**) projection of $Bi_{26}Mo_{10}O_{\delta}$; (b) $[Bi_{12}O_{14}]$ roses in $\gamma' Bi_2MoO_6$.

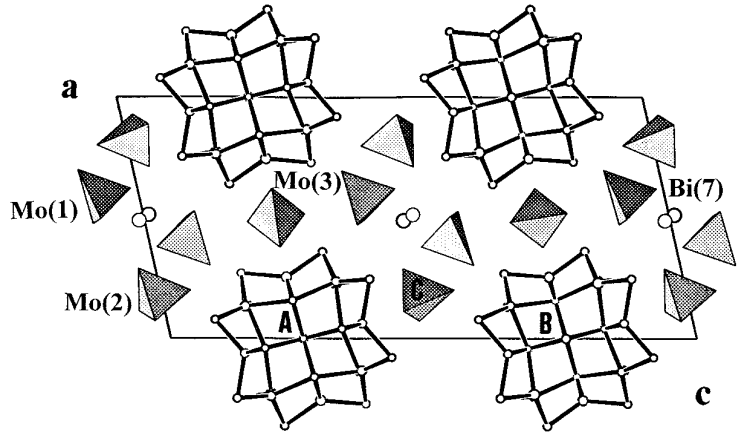

a)

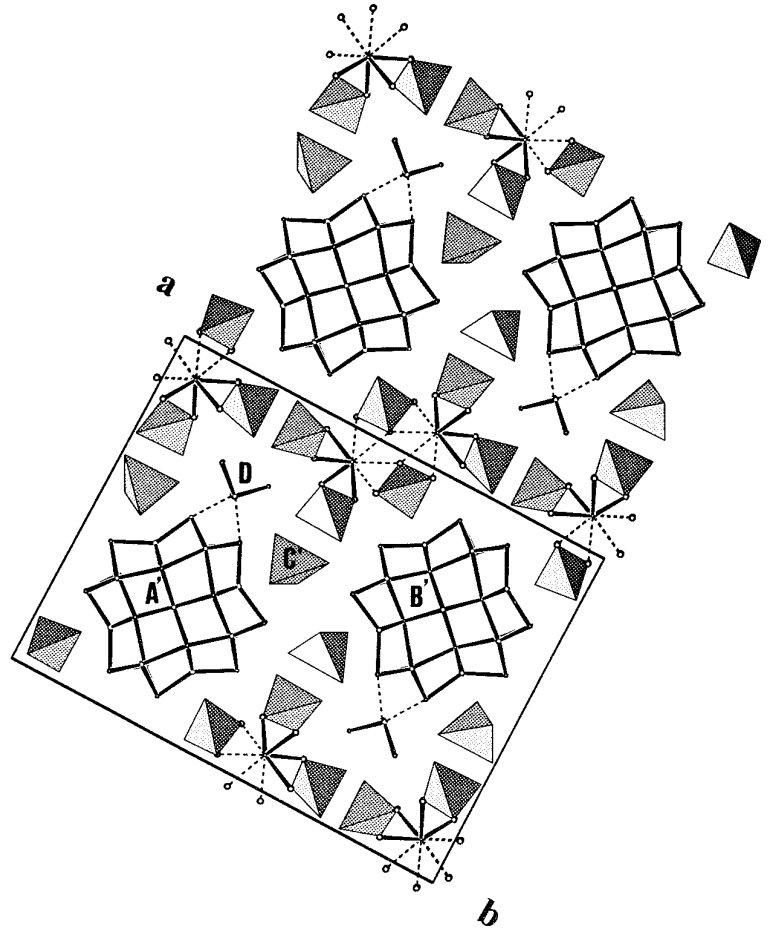

b)

FIG. 3. (a) (**a, c**) projection of $Bi_{26}Mo_{10}O_{\delta}$ structure; (b) (**a, b**) projection of $\gamma'Bi_2MoO_6$ structure.

TABLE 1
Crystal Data, Intensity Measurement, and Structure Refinement Parameters

	$Bi_{26}Mo_{10}O_{\delta}$		$Bi_{26}Mo_6V_4O_{\delta}$	
	Crystal data			
Crystal symmetry	Monoclinic		Monoclinic	
Space group	$P2/c$		$P2/c$	
Cell dimension	a = 11.742(8) Å		a = 11.633(7) Å	
	b = 5.800(7) Å		b = 5.795(3) Å	
	c = 24.77(5) Å		c = 24.39(2) Å	
	β = 102.94(6)°		β = 101.35(5)°	
Z	1		1	
	Data collection			
Equipment	Philips PW 1100		Philips PW 1100	
λ (Mo$K\alpha$ (graphite monoch.))	0.7107 Å		0.7107 Å	
Scan mode	$\omega - 2\theta$		$\omega - 2\theta$	
Scan width	1.2°		1.2°	
θ range	2°–25°		2°–25°	
Standard reflections measured every 2 hr	−2 0 0, 2 0 2, 1 −4 −2		0 −2 0, −2 0 −4, −3 2 −4	
Recording reciprocal space	$-13 \le h \le 13$, $0 \le k \le 6$, $-29 \le l \le 29$		$-13 \le h \le 13$, $0 \le k \le 6$, $-29 \le l \le 29$	
Number of measured reflections	5168		6276	
Number of reflections $I > 3\sigma(I)$	4242		3614	
Number of independent reflections	2229		1922	
μ	680 cm^{-1}		625 cm^{-1}	
Limiting faces and distances from an arbitrary origin	0 1 0	100 μm	−1 0 0	36 μm
	1 0 0	57.5 μm	1 0 0	36 μm
	−1 0 0	57.5 μm	1 1 0	132 μm
	0 0 1	17 μm	−4 −7 0	126 μm
	0 0 −1	17 μm	0 0 1	19.5 μm
	0 −1 1	91 μm	0 0 −1	19.5 μm
Transmission factor range	0.011–0.116		0.018–0.118	
Merging R factor	0.054		0.039	
	Refinement			
Number of refined parameters	156		159	
$R = \Sigma(\|F_0\| - \|F_c\|)/\|F_0\|$	0.048		0.041	
$R_w = [\Sigma w(\|F_0\| - \|F_c\|)^2/\Sigma F_0^2]^{1/2}$ with $w = 1/\sigma(F_0)$	0.060		0.047	

15 sec counting time. A Philips PW 1100 diffractometer was used for single crystal data collection.

DSC measurements were made by means of a Dupont Instrument 910 with a gold cell in air, up to 570°C with a scanning rate of 10°C/min on heating and on cooling.

Density measurements were carried out using a Micromeritics Accupyc 1330 helium pycnometer, 1 ml sample capacity.

Conductivity measurements were performed with sintered pellets using impedance spectroscopy (Solartron 1170 frequency response analyzer) in the frequency range from 1 to 10^6 Hz. Measurements were made from 200 to 840°C by steps of 20°C with 60 min stabilization time. No significant difference, within the experimental uncertainty, was observed between the heating and cooling cycles and the reported results correspond to the second heating cycle.

Single crystals containing vanadium were found in the melt cooled from 900 to 800°C with a 2°C/hr rate.

Bismuth molybdenum oxide single crystals were obtained from a melt of $3Bi_2O_3$–$2MoO_3$ nominal composition, cooled from 1000 to 900°C with a 2°C/hr rate. The composition of both crystals were deduced from the resolution of their structures and yielded $Bi_{26}Mo_6V_4O_{67}$ and $Bi_{26}Mo_{10}O_{69}$, respectively.

STRUCTURE REFINEMENT AND DISCUSSION

Structure determination was carried out in the same way for both crystals. Preliminary oscillation and Weissenberg photographs revealed $2/m$ Laüe symmetry combined with systematic absence of $h0l$ ($l = 2n$) reflections, characterizing the $P2/c$ space group. Data collection conditions are

TABLE 2a
Positional Parameters Corresponding to $Bi_{26}Mo_{10}O_{\delta}$

Atom	Site	Occupancy factor	x	y	z	B or B_{eq} (Å^2)
Bi(1)	4g	1	0.04101(8)	0.4163(2)	0.32690(5)	0.99(3)
Bi(2)	4g	1	0.15779(8)	0.9151(2)	0.24587(5)	1.06(3)
Bi(3)	4g	1	0.24670(8)	0.0113(2)	0.40065(4)	1.20(3)
Bi(4)	4g	1	0.36084(7)	0.5026(2)	0.32328(5)	1.19(3)
Bi(5)	4g	1	0.26942(7)	0.5034(2)	0.16025(5)	1.07(3)
Bi(6)	4g	1	0.07778(7)	0.0081(2)	0.09138(4)	1.03(3)
Bi(7)	4g	0.5	0.5120(7)	0.478(2)	0.0101(2)	3.5(2)
Mo(1)	4g	1	0.4180(2)	−.0045(5)	0.0775(2)	1.54(6)
Mo(2)	4g	1	0.8317(3)	0.5160(5)	0.0108(2)	2.06(7)
Mo(3)	2f	1	½	0.0078(8)	¼	1.83(9)
O(1)	2e	1	0	0.727(4)	¼	0.9(4)
O(2)	4g	1	0.136(2)	0.261(3)	0.1582(8)	1.3(3)
O(3)	4g	1	0.132(2)	0.755(4)	0.1539(9)	1.7(4)
O(4)	4g	1	0.238(2)	0.769(3)	0.3362(8)	1.4(4)
O(5)	4g	1	0.255(2)	0.589(4)	0.2440(8)	1.6(3)
O(6)	4g	1	0.063(2)	0.066(3)	0.3674(8)	1.3(3)
O(7)	2e	1	0	0.239(5)	¼	1.4(5)
O(8)	4g	1	0.230(2)	0.269(4)	0.3350(9)	1.7(4)
O(9)	4g	1	0.506(3)	−0.265(8)	0.082(2)	9(1)
O(10)	4g	1	0.379(4)	0.106(9)	0.013(3)	11(2)
O(11)	4g	1	0.302(4)	−0.024(8)	0.105(2)	9(2)
O(12)	4g	1	0.528(4)	0.205(9)	0.099(3)	12(2)
O(13)	4g	1	0.929(3)	0.303(8)	0.023(2)	9(1)
O(14)	4g	1	0.800(3)	0.552(6)	−0.058(2)	6.0(7)
O(15)	4g	1	0.888(3)	0.755(6)	0.049(2)	6.7(8)
O(16)	4g	1	0.710(3)	0.433(6)	0.032(2)	6.9(8)
O(17)	4g	1	0.378(2)	0.166(5)	0.245(2)	4.3(5)
O(18)	4g	1	0.482(4)	−0.180(9)	0.194(3)	11(2)

Anisotropic temperature coefficient ($Bi_{26}Mo_{10}O_{\delta}$)

Atom	U_{11}	U_{22}	U_{33}	U_{12}	U_{13}	U_{23}
Bi(1)	0.0129(6)	0.0123(6)	0.0129(5)	0.0004(4)	0.0041(4)	−0.0014(4)
Bi(2)	0.0114(5)	0.0106(6)	0.0195(6)	0.0002(4)	0.0063(4)	−0.0004(5)
Bi(3)	0.0190(5)	0.0135(5)	0.0132(6)	0.0022(4)	0.0039(4)	0.0010(5)
Bi(4)	0.0099(4)	0.0151(5)	0.0204(6)	0.0002(5)	0.0042(4)	−0.0024(5)
Bi(5)	0.0094(4)	0.0155(5)	0.0166(5)	0.0017(4)	0.0051(4)	0.0044(5)
Bi(6)	0.0144(5)	0.0136(5)	0.0110(5)	−0.0022(4)	0.0034(4)	0.0003(5)
Bi(7)	0.040(3)	0.074(4)	0.023(4)	0.004(3)	0.015(3)	0.000(3)
Mo(1)	0.0120(9)	0.019(2)	0.029(2)	−0.0014(9)	0.0082(9)	0.001(2)
Mo(2)	0.041(2)	0.020(2)	0.017(2)	0.002(2)	0.005(2)	0.002(2)
Mo(3)	0.019(2)	0.019(2)	0.032(3)	0	0.005(2)	0

given in Table 1. The intensity of each reflection was corrected for background, Lorentz-polarization effects, and absorption using the analytic method of De Meulenaer and Tompa (12). Bismuth atoms were first localized by direct methods and successive Fourier difference enabled us to determine the remaining atomic positions. Anomalous dispersion coefficients from Cromer and Liberman (13) were used in the least-squares refinement. In the Bi–(Mo,V) structure, Mo and V atoms were localized on the same sites and the Mo/V ratio were refined, leading to a $Bi_{26}Mo_6V_4O_{\delta}$ formulation. The final positional and atomic displacement parameters are presented in Table 2a and 2b.

The structural similitude of these crystals is clearly evidenced, and the Bi–Mo mixed oxide will be used for discussion.

(**a, b**), (**b, c**), and (**a, c**) projections are represented in Figs. 1, 2, and 3. Projection along the twofold axis reveals a ''rose'' built up from Bi(1)–(6) and O(1)–(8) atoms, yielding a $[Bi_{12}O_{14}]_{\infty}$ network (Figs. 4 and 5), extending along the twofold axis. These columns display a clear cova-

TABLE 2b
Positional Parameters Corresponding to $Bi_{26}Mo_6V_4O_{\delta}$

Atom	Site	Occupancy factor	x	y	z	B or B_{eq} (Å^2)
Bi(1)	4*g*	1	0.03800(8)	0.4128(2)	0.32736(5)	0.89(3)
Bi(2)	4*g*	1	0.15857(8)	0.9101(2)	0.24508(5)	1.02(3)
Bi(3)	4*g*	1	0.23743(8)	0.0047(3)	0.40059(4)	1.28(3)
Bi(4)	4*g*	1	0.35916(7)	0.4960(3)	0.32079(5)	1.20(3)
Bi(5)	4*g*	1	0.27319(7)	0.4962(3)	0.15770(5)	1.33(3)
Bi(6)	4*g*	1	0.08283(8)	0.0009(3)	0.08970(4)	1.16(3)
Bi(7)	4*g*	0.5	0.510(2)	0.502(5)	0.0076(5)	2.6(3)
Mo,V(1)	4*g*	0.58/0.42(3)	0.4272(3)	−.0076(7)	0.0794(2)	1.54(8)
Mo,V(2)	4*g*	0.68/0.32(2)	0.8309(3)	0.5131(7)	0.0126(2)	1.22(8)
Mo,V(3)	2*f*	0.55/0.45(4)	½	0.007(2)	¼	1.9(2)
O(1)	2*e*	1	0	0.719(5)	¼	1.3(5)
O(2)	4*g*	1	0.140(2)	0.253(3)	0.1521(9)	1.0(3)
O(3)	4*g*	1	0.136(2)	0.744(4)	0.1521(9)	2.0(4)
O(4)	4*g*	1	0.237(2)	0.763(3)	0.3359(8)	1.6(4)
O(5)	4*g*	1	0.254(2)	0.581(4)	0.2420(8)	1.9(4)
O(6)	4*g*	1	0.059(2)	0.054(3)	0.3670(8)	1.6(4)
O(7)	2*e*	1	0	0.232(4)	¼	1.0(5)
O(8)	4*g*	1	0.229(2)	0.264(3)	0.3352(8)	1.1(4)
O(9)	4*g*	1	0.496(3)	−0.273(6)	0.079(2)	6.0(7)
O(10)	4*g*	1	0.379(4)	0.067(9)	0.011(3)	13(2)
O(11)	4*g*	1	0.312(3)	−0.012(6)	0.108(2)	6.3(7)
O(12)	4*g*	1	0.527(4)	0.195(8)	0.097(2)	10(2)
O(13)	4*g*	1	0.919(3)	0.287(6)	0.032(2)	3.3(5)
O(14)	4*g*	1	0.803(2)	0.544(5)	−0.056(2)	4.4(6)
O(15)	4*g*	1	0.894(2)	0.754(4)	0.048(1)	3.4(5)
O(16)	4*g*	1	0.700(2)	0.452(5)	0.038(2)	4.4(6)
O(17)	4*g*	1	0.378(2)	0.168(5)	0.246(2)	4.4(6)
O(18)	4*g*	1	0.483(5)	−0.17(2)	0.199(3)	17(2)

Anisotropic temperature coefficient ($Bi_{26}Mo_6V_4O_{\delta}$)

Atom	U_{11}	U_{22}	U_{33}	U_{12}	U_{13}	U_{23}
Bi(1)	0.0145(5)	0.0099(5)	0.0089(6)	0.0007(4)	0.0011(4)	−0.0011(4)
Bi(2)	0.0137(5)	0.0099(5)	0.0153(6)	−0.0001(4)	0.0027(4)	−0.0006(5)
Bi(3)	0.0199(5)	0.0148(5)	0.0117(5)	0.0025(6)	−0.0026(4)	−0.0009(6)
Bi(4)	0.0109(4)	0.0144(5)	0.0189(6)	0.0000(6)	−0.0008(4)	−0.0045(7)
Bi(5)	0.0120(5)	0.0180(5)	0.0214(6)	0.0025(6)	0.0055(4)	0.0055(7)
Bi(6)	0.0198(5)	0.0147(5)	0.0099(5)	−0.0033(6)	0.0041(4)	−0.0008(6)
Bi(7)	0.043(5)	0.037(2)	0.017(6)	−0.002(4)	0.004(4)	−0.008(6)
Mo,V(1)	0.014(2)	0.025(2)	0.021(2)	−0.000(2)	0.005(2)	−0.004(2)
Mo,V(2)	0.025(2)	0.015(2)	0.007(2)	0.001(2)	0.002(2)	0.001(2)
Mo,V(3)	0.014(3)	0.015(3)	0.043(4)	0	0.009(2)	0

lent character (14) and the constituting atoms are associated with low thermal coefficients. Bi atoms exhibit the usual one-sided variable coordination characterizing the Bi^{3+} cation and its stereochemically active $6s^2$ lone pair: 4 or 3 short Bi–O bond lengths (<2.4 Å) and variable additional larger ones (Fig. 5, Table 3). The Bi–O short distances always involve O atoms labeled O(1) to O(8) which belong to the $[Bi_{12}O_{14}]_{\infty}$ network.

These $[Bi_{12}O_{14}]_{\infty}$ columns are connected with MoO_4 or (Mo, V)O_4 tetrahedra. Six of these tetrahedra, based on Mo(1) and Mo(2) type atoms, surround the isolated Bi(7) atom coordinated with 8 O atoms (Fig. 6). The coordination of this Bi(7) is very particular since 4 out of the 8 oxygen atoms labeled as O(9) and O(16) are in a planar configuration, and Bi(7) is only 0.20(1) Å off this plane in $Bi_{26}Mo_{10}O_{\delta}$ and 0.05(3) Å in $Bi_{26}Mo_6V_4O_{\delta}$! Such a flat square, or rectangular Bi–O_4 pyramid is rather unusual but has recently been observed in a bismuth hollandite-type compound $Bi_{1.7}V_8O_{16}$ (15) with a 0.30 Å distance for Bi off the square plane O_4.

We must notice that, during the determination of the structures, this Bi(7) atom appeared localized on a center

TABLE 3
Bond Lengths Corresponding to $Bi_{26}Mo_{10}O_\delta$ and $Bi_{26}Mo_6V_4O_\delta$ in Å

		$Bi_{26}Mo_{10}O_\delta$	$Bi_{26}Mo_6V_4O_\delta$			$Bi_{26}Mo_{10}O_\delta$	$Bi_{26}Mo_6V_4O_\delta$
Bi(1)	—O(1)	2.59(2)	2.56(2)	Bi(2)	—O(1)	2.17(2)	2.17(2)
	—O(2)	2.37(3)	2.41(3)		—O(2)	2.92(2)	2.99(2)
	—O(3)	2.94(3)	2.90(3)		—O(3)	2.41(3)	2.43(3)
	—O(4)	3.06(3)	3.05(3)		—O(4)	2.38(2)	2.38(2)
	—O(6)	2.25(2)	2.29(2)		—O(5)	2.22(2)	2.21(3)
	—O(7)	2.12(2)	2.13(2)		—O(7)	2.66(3)	2.64(2)
	—O(8)	2.34(3)	2.36(3)		—O(8)	2.99(3)	3.00(2)
valence sum		3.0	3.0		—O(17)	2.97(3)	2.95(3)
				valence sum		2.9	2.9
Bi(3)	—O(4)	2.11(2)	2.11(2)				
	—O(6)	2.15(3)	2.10(3)	Bi(4)	—O(4)	2.19(3)	2.18(3)
	—O(8)	2.18(3)	2.18(5)		—O(5)	2.13(2)	2.12(2)
	—O(10)	2.95(7)	2.90(7)		—O(8)	2.12(3)	2.11(3)
	—O(12)	2.89(5)	2.94(5)		—O(9)	2.86(5)	3.00(4)
	—O(15)	2.68(5)	2.60(3)		—O(12)	2.72(6)	2.79(5)
	—O(16)	2.94(4)	3.01(4)		—O(17)	2.79(5)	2.67(4)
valence sum		3.1	3.4		—O(18)	2.71(6)	2.8(1)
				valence sum		3.3	3.3
Bi(5)	—O(2)	2.10(3)	2.08(3)				
	—O(3)	2.16(3)	2.13(3)	Bi(6)	—O(2)	2.20(2)	2.12(2)
	—O(5)	2.18(3)	2.17(3)		—O(3)	2.13(3)	2.13(3)
	—O(14)	2.50(5)	2.48(5)		—O(6)	2.15(3)	2.15(3)
	—O(17)	2.94(4)	2.95(4)		—O(11)	2.58(5)	2.62(3)
valence sum		3.3	3.4		—O(13)	2.74(5)	2.70(4)
					—O(15)	2.68(4)	2.65(3)
Bi(7)	—O(9)	2.56(5)	2.48(5)	valence sum		3.2	3.3
	—O(9)	2.34(5)	2.21(5)				
	—O(10)	2.67(6)	2.95(6)	Mo(V)(1)	—O(9)	1.81(5)	1.73(4)
	—O(10)	2.85(6)	2.89(6)		—O(10)	1.69(7)	1.71(7)
	—O(12)	2.69(7)	2.79(6)		—O(11)	1.66(6)	1.63(4)
	—O(12)	3.22(7)	3.06(6)		—O(12)	1.75(5)	1.65(5)
	—O(16)	2.28(4)	2.21(4)		—O(18)	2.99(7)	3.01(8)
	—O(16)	2.63(4)	2.49(4)	valence sum		6.6	6.8
valence sum		2.2	2.6				
				Mo(V)(3)	—O(17)	1.68(3)(×2)	1.68(3)(×2)
Mo(V)(2)	—O(13)	1.66(5)	1.67(4)		—O(18)	1.74(7)(×2)	1.6(1)(×2)
	—O(14)	1.67(5)	1.66(5)	valence sum		6.8	7.4
	—O(15)	1.72(4)	1.73(3)				
	—O(16)	1.70(5)	1.79(4)				
valence sum		7.3	6.2				

Note. Valence sums are calculated using the method of Brown and Shannon (16) and the data of Brown and Altermatt (17) ($V_j = \Sigma_j \exp((r_0 - r_{ij})/0.37)$) with $r_0(\mathrm{Bi}) = 2.094$, $r_0(\mathrm{Mo}) = 1.907$, $r_0(\mathrm{Mo,V}) = 0.6 \times 1.907 + 0.4 \times 1.803 = 1.865$).

TABLE 4
Cell Parameters in Å Refined on Powder Diffraction Data Corresponding to $Bi_xMo_{10}O_\delta$

x	a	b	c	α	β	γ	V(Å^3)	d^a_{th}	d_{exp}
25.75	11.793(3)	5.807(2)	24.726(6)	89.87(2)	102.71(2)	89.92(2)	1652(2)		7.52
26	11.800(4)	5.808(2)	24.744(8)	89.85(2)	102.76(2)	89.97(2)	1654(2)	7.53 ($y = 0$)	7.54
27	11.771(3)	5.801(2)	24.772(6)	89.96(2)	102.91(2)	89.93(2)	1649(2)	7.58 ($y = 0.27$)	7.57
27.5	11.741(3)	5.800(2)	24.782(6)	90	102.81(2)	90	1646(2)	7.60 ($y = 0.40$)	7.63
27.75	11.740(1)	5.798(1)	24.793(3)	90	102.90(1)	90	1645(2)	7.61 ($y = 0.46$)	7.61

[a] Assuming a $Bi_{26}Mo_{10-y}Bi_yO_{69-1.5y}$ unit per cell.

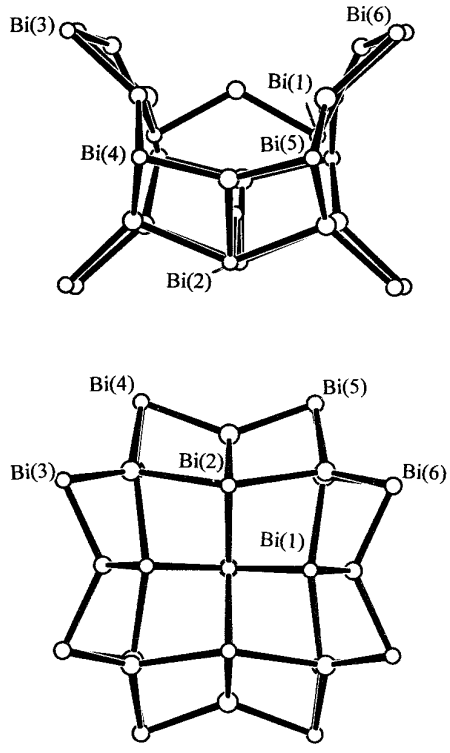

FIG. 4. $[Bi_{12}O_{14}]$ rose.

of symmetry ($2b$ site of $P2/c$ space group) which is not suitable for a cation with an electronic lone pair $6s^2$. Refinement on this site led to abnormally high B values and thereby the Bi(7) cation was splitted on a $4g$ type site with an occupation ratio = 0.5 leading to more acceptable B values.

The Mo(3)-type MoO_4 tetrahedra are not involved in the Bi(7) coordination but a common feature to all the Mo–O_4 (or Mo, V–O_4) tetrahedra is the high observed B values of all their O atoms labeled as O(9) to O(18) in Table 2. This behavior, which is a classical one in crystal structures containing tetrahedral entities smoothly bonded to cations or covalent skeleton, is likely to be due to large individual vibrations of the O atoms around the center of mass (Mo atom) or librations of the tetrahedra considered as rigid-body species. Both models lead to apparent shortening of the Mo–O bond lengths within Mo(1)-, Mo(2)-, and Mo(3)-based MoO_4 tetrahedra, and thereby to lengthening of the Bi(7)–O distances. This can explain the overestimated Mo–O and (Mo, V)–O, and the underestimated Bi(7)–O, valence sums calculated according to the method of Brown and Shannon (16) with the data from Brown and Altermatt (17).

The crystal structure determinations enabled us to obtain the formulation of the crystals. With the Bi–Mo mixed oxide, we obtain $Bi_{26}Mo_{10}$ per unit cell for the cationic content. Assuming Bi^{III} and Mo^{VI} valence states, we should find a $Bi_{26}Mo_{10}O_{69}$ formulation but the O crystallographic sites, $16 \times 4g$ plus $2 \times 2e$, lead to $Bi_{26}Mo_{10}O_{68}$ and there would have one O missing, undetected in the crystal structure determination.

In the Bi–Mo, V mixed oxide, we obtain $Bi_{26}Mo_6V_4$, and using the same assumption of Bi^{III}, Mo^{VI}, and V^{V} valence states, the formulation should be $Bi_{26}Mo_6V_4O_{67}$, while the crystal structure determination yields $Bi_{26}Mo_6V_4O_{68}$ with the O sites, and this time one O in excess.

Classical physical analytical methods such as EDAX or thermogravimetry under reducing atmosphere are not accurate enough to determine the oxygen stoichiometry of these crystals but we can consider the results obtained from single crystal X-ray diffraction data as unambiguous for the cationic contents and acceptable for the oyxgen amount. The last point will be further discussed later on with the problem of the solid solution.

When compared with the high-temperature γ' polymorph of Bi_2MoO_6 recently determined from neutron powder diffraction, striking similar structural features appear (Figs. 2 and 3). The $[Bi_{12}O_{14}]$ moiety of $Bi_{26}Mo_{10}O_{\delta}$ and $Bi_{26}Mo_6V_4O_{\delta}$, is in fact a predominant part of the so-called "latin cross" in $\gamma'Bi_2MoO_6$(2). The $Bi_{12}O_{14}$ rose displays the same geometry, the same dimensions, and the same thickness in both cases. The latin cross in Bi_2MoO_6 is obtained from the $Bi_{12}O_{14}$ rose by linking Bi_2O_2 chains (D) to form the foot of the cross. Moreover, it is worthwhile to notice that the A and B roses and C (Mo(2) type) tetrahedra in $Bi_{26}Mo_{10}O_{\delta}$ superimpose with the A' and B' roses and C' tetrahedra in Bi_2MoO_6. This last point will also be used to discuss the problem of the solid solution.

THE SOLID SOLUTION $Bi_xMo_{10}O_{\delta}$

The possibility to substitute some VO_4 tetrahedra for MoO_4 tetrahedra is not surprising owing to the close dimensional similitude between these moieties, but a solid solution domain around $Bi_{26}Mo_{10}O_{\delta}$ in the binary diagram Bi_2O_3–MoO_3 is more puzzling owing to the structural characteristics described above. Such a solid solubility was previously proposed by several authors (6, 7) and we reexamined this part of the diagram. The solid solution, if any, could be formally written as $Bi_xMo_{10}O_{\delta}$ and samples corresponding to different x values were prepared at 850°C and quenched in air: x = 20 (γBi_2MoO_6), 24, 25, 25.5, 25.75, 26, 27, 27.5, 27.75, 28, 29, 30 ($3Bi_2O$–$2MoO_3$), 33, and 40.

Typical X-ray powder diffraction patterns are reported in Fig. 7. Clearly, a solid solution is observed within the range $25.75 \leq x \leq 27.75$. Compositions below x = 25.75 exhibit a two phase mixture of $\gamma'Bi_2MoO_6$ and x = 25.75, while beyond x = 27.75 a mixture made of x = 27.75 and $Bi_{38}Mo_7O_{78}$ (10) is identified. With our experimental conditions, we can therefore point out that $3Bi_2O_3$–

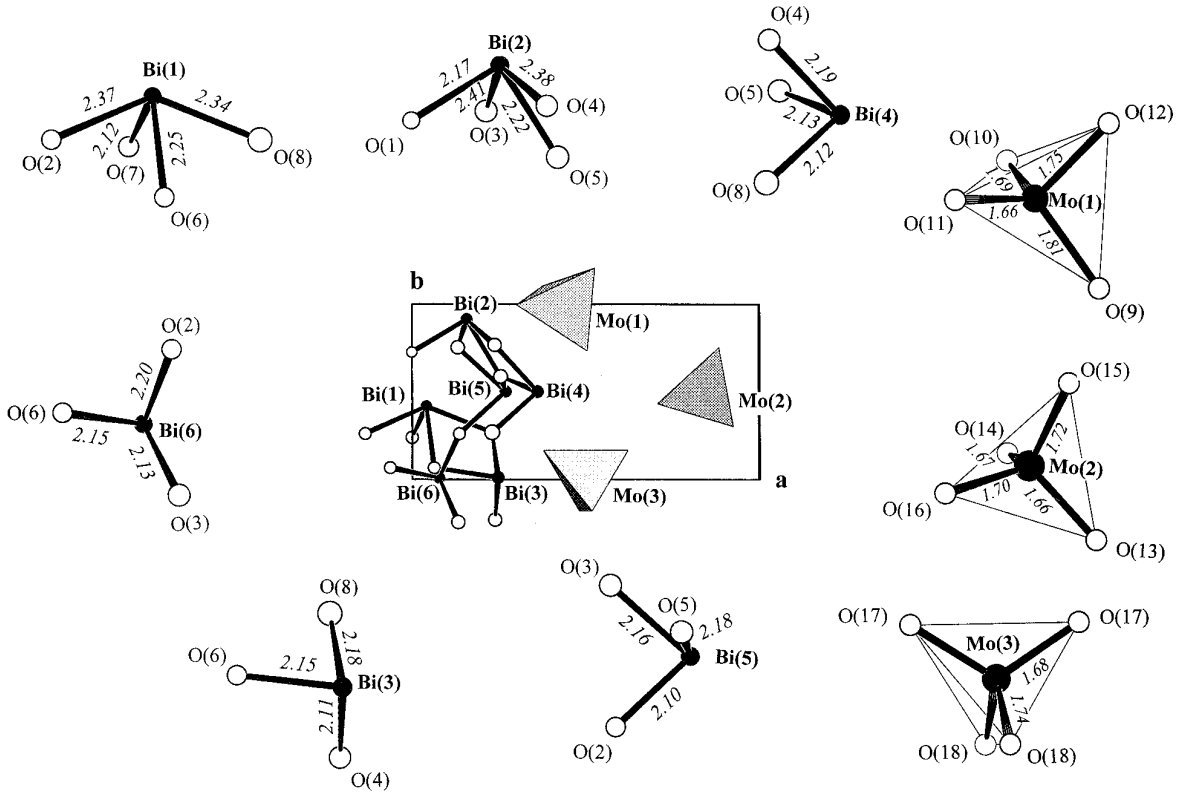

FIG. 5. Bi(1)–Bi(6) and Mo surroundings.

$2MoO_3$, usually described as a defined compound (11, 8, 9), is a two phase mixture.

Within the solid solution, $x = 27.75$ and $x = 27.50$ compositions have a monoclinic symmetry, while this symmetry becomes triclinic for smaller x contents. The unit cell parameters characterizing some compositions have been determined and are reported in Table 4. An apparent discrepancy occurs between the $Bi_{26}Mo_{10}O_\delta$ single crystal previously described in the monoclinic $P2/c$ space group, and the triclinic symmetry determined from powder diffraction with the same formulation. We believe that the monoclinic phase is the high-temperature polymorph of the room temperature triclinic phase. The single crystal used for crystal structure determination was a quenched phase, a classical behavior observed when the phase transition temperature is akin to the ambient temperature. This hypothesis is corroborated by two experimental observations.

—A high temperature X-ray diffraction pattern (Fig. 8) performed on powder $Bi_{26}Mo_{10}O_\delta$ clearly reveals a reversible phase transition at about 310°C, corresponding to a triclinic ↔ monoclinic transformation.

—DSC measurements carried out on the same composition exhibit a thermal effect (Fig. 9) at about 310°C, while nothing is observed on $x = 27.50$.

Miyazawa *et al.* (11), using dilatometry, previously reported a phase transition occurring near 280°C, for their crystal corresponding, as indicated here above, to the same compound.

In addition to the $Bi_xMo_{10}O_\delta$ range in the Bi_2O_3–MoO_3 system, some Mo → V substitutions have been performed along the $Bi_{26}Mo_{10-y}O_\delta$ and $Bi_{27}Mo_{10-y}O_\delta$ lines within the Bi_2O_3–MoO_3–V_2O_5 ternary diagram. The compositional limits of the same structure-type solid solution are reported on Fig. 10. A maximum $y = 4$ value was obtained on both

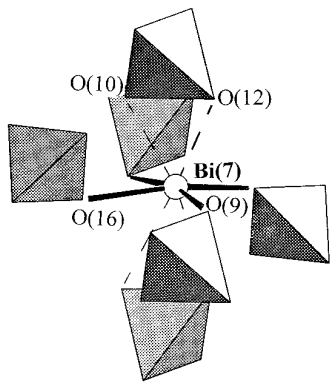

FIG. 6. Bi(7) surrounding.

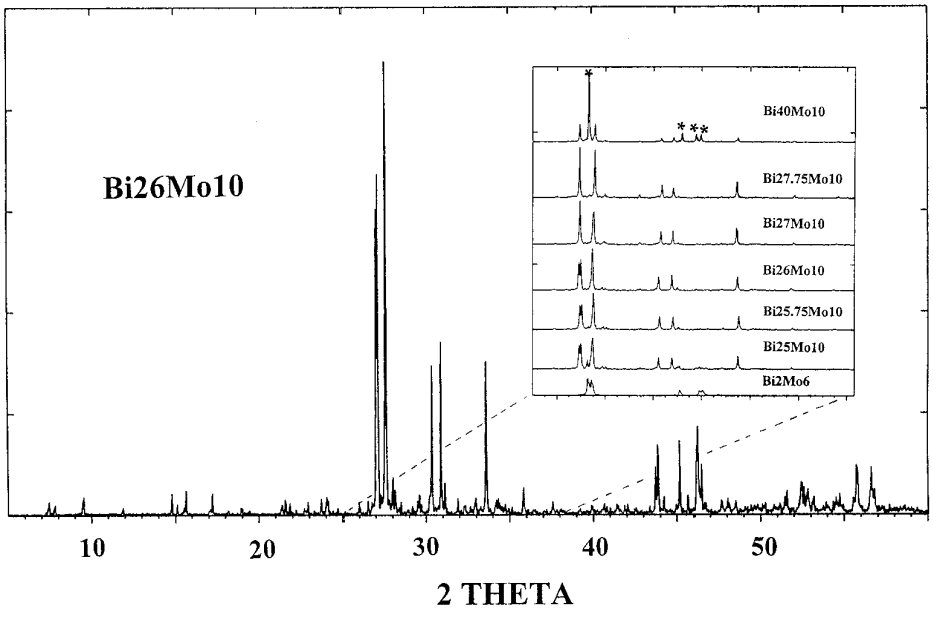

FIG. 7. X-ray diffraction patterns (* correspond to $Bi_{38}Mo_7O_{78}$ lines).

lines, and introduction of at least 10% of vanadium in molybdenum site leads to the stabilization of a monoclinic phase at room temperature. The unit cell parameters of these compounds are reported in Table 5.

Density measurements have been performed on some compounds and are presented in Table 5. For a given Bi/(Mo + V) ratio, the experimental values are in accordance with the substitution for molybdenum with vanadium, as revealed in the $Bi_{26}Mo_6V_4O_{\delta}$ crystal structure determination. When $y = 0$ ($Bi_xMo_{10}O_{\delta}$ line) (Table 4), the experi-

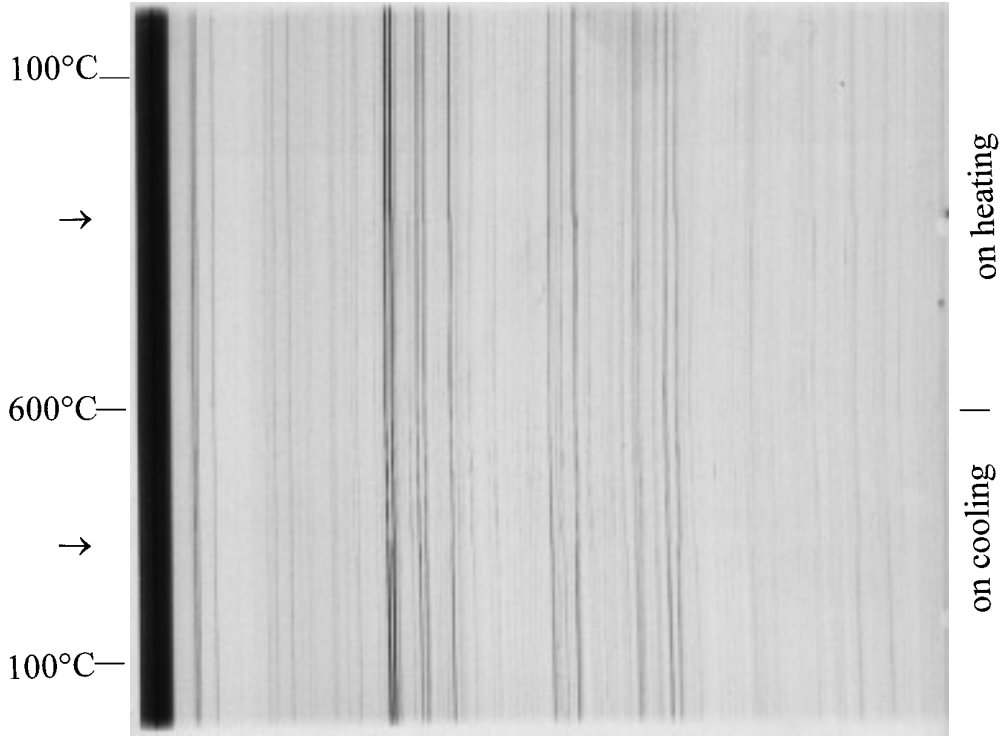

FIG. 8. HTXRD corresponding to $Bi_{26}Mo_{10}O_{\delta}$ powder.

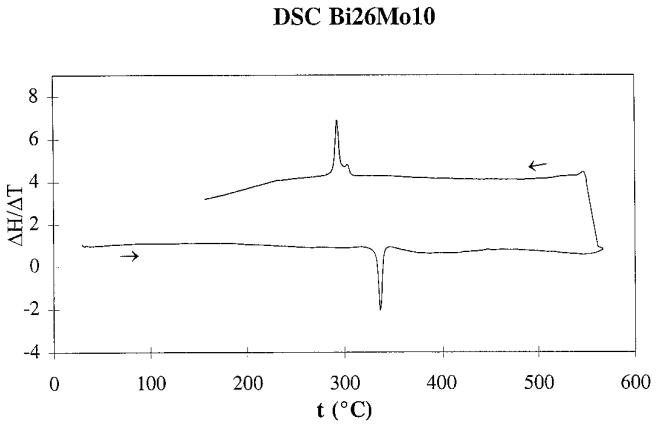

FIG. 9. DSC corresponding to $Bi_{26}Mo_{10}O_{\delta}$ powder.

mental values are in agreement with the hypothesis of bismuth substituting for molybdenum and therefore a solid solution written as $Bi_{26}(Mo_{10-y}Bi_y)O_{\delta}$ instead of $Bi_xMo_{10}O_{\delta}$. With $x = 25.75$, the bismuth vacancy hypothesis gives a good agreement.

Combining these experimental density data with the structural features characterizing the $Bi_{26}Mo_{10}O_{\delta}$ structure, it is possible to try and propose some mechanisms to explain this type of solid solution and to understand the stoichiometric problems dealing with the oxygen content. The basic cationic composition will be $Bi_{26}Mo_{10}$ in the following discussion.

Toward the lower x limit of $Bi_xMo_{10}O_{\delta}$ solid solution, the crystallographic defect of one O atom of $Bi_{26}Mo_{10}O_{\delta}$, as mentioned above, could be for instance the result of electrical compensation if some Mo^V was present. The absence of any EPR signal characterizing the paramagnetic Mo^V cation rules out this mechanism.

On the other hand, toward the upper x limit, increasing the Bi/Mo ratio from the crystallographic Bi/Mo = 26/10 is not possible by simple substitution for Mo with Bi. All the Mo atoms are tetrahedraly coordinated with O atoms and this coordination is not acceptable for a Bi^{3+} cation. We rather propose a mechanism suggested by the comparison of the $Bi_{26}Mo_{10}O_{\delta}$ and $\gamma'Bi_2MoO_6$ crystal structures.

As mentioned here above, the latin cross of Bi_2MoO_6 is made of the $[Bi_{12}O_{14}]$ moiety characterizing $Bi_{26}Mo_{10}O_{\delta}$, completed with Bi_2O_2 chains extending along the twofold axis (Fig. 3b), and these Bi_2O_2 chains in Bi_2MoO_6 occupy the same domain, between the $[Bi_{12}O_{14}]_{\infty}$ columns, as do the isolated Bi(7) and one MoO_4 tetrahedron in $Bi_{26}Mo_{10}O_{\delta}$. We can easily imagine that additional Bi atoms, corresponding to Bi/Mo > 26/10, could substitute for an equivalent amount of MoO_4 tetrahedra. This substitution would lead to transformation of some $[Bi_{12}O_{14}]_{\infty}$ roses into some $[Bi_{12}O_{14}, Bi_2O_2]$ latin cross parts in the $[Bi_{12}O_{14}]_{\infty}$ network of the structure, without significant volume change of the unit cell, as experimentally observed in Table 4. This hypothesis accounts for the results obtained using different techniques: unit cell parameters, densities, chemical compositions, etc., and moreover enlightens the correlation between the crystal structures of $Bi_{26}Mo_{10}O_{\delta}$ on one hand and $\gamma'Bi_2MoO_6$ on the other. $Bi_{26}Mo_{10}O_{\delta}$ could be formulated as $[Bi_{12}O_{14}](MoO_4, Bi)$, $4MoO_4$ to be compared with $\gamma'Bi_2MoO_6$ expressed as $[Bi_{12}O_{14}](Bi_2O_2)$, 2Bi,

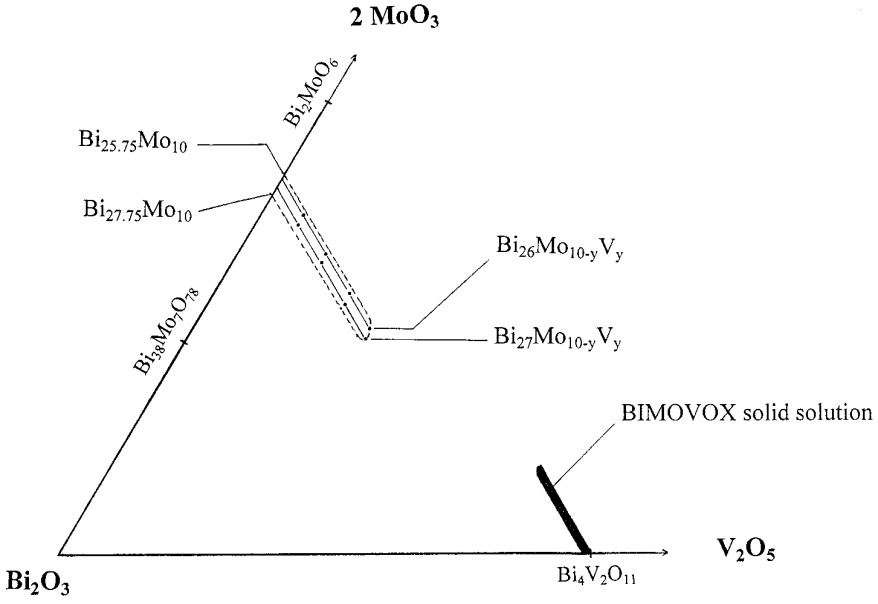

FIG. 10. $Bi_{26}Mo_{10}O_{\delta}$ solid solution type in the Bi_2O_3–MoO_3-V_2O_5 ternary diagram.

TABLE 5
Cell Parameters Refined on Powder Diffraction Data

y	a	b	c	α	β	γ	V(Å^3)	d_{th}	d_{exp}
				$Bi_{26}Mo_{10-y}V_yO_\delta$					
1	11.709(3)	5.801(2)	24.646(5)	90	101.69(2)	90	1639(2)	7.54[a]	7.55
2	11.694(5)	5.802(2)	24.502(7)	90	101.28(2)	90	1630(2)	7.53[a]	7.57
3	11.639(5)	5.796(2)	24.425(6)	90	101.32(2)	90	1616(2)	7.54[a]	7.56
4	11.620(1)	5.801(1)	24.382(2)	90	101.43(2)	90	1611(2)	7.51[a]	7.53
				$Bi_{27}Mo_{10-y}V_yO_\delta$					
1	11.702(3)	5.797(2)	24.657(6)	90	102.09(2)	90	1636(2)	7.59[b]	7.53
2	11.678(3)	5.793(2)	24.538(5)	90	101.66(2)	90	1626(2)	7.58[b]	7.58
3	11.654(2)	5.797(1)	24.466(3)	90	101.51(1)	90	1620(2)	7.56[b]	7.58
4	11.630(2)	5.798(1)	24.416(3)	90	101.51(1)	90	1613(2)	7.53[b]	7.57

[a] Assuming a $Bi_{26}(Mo_yV_{10-y})O_{64+0.5y}$ unit per cell.
[b] Assuming a $Bi_{26}Mo_{9.73-x}Bi_{0.27}V_xO_{68.595-0.5x}$ unit per cell.

$8MoO_4$. The part between brackets [ ] describe the common rose unit, and that between parentheses ( ), the part suitable for MoO_4/Bi substitution. Further experiments such as neutron diffraction are in progress to determine the actual oxygen stoichiometry of these compounds.

CONDUCTIVITY MEASUREMENTS

Takahashi *et al.* (18) on one hand, and Boon and Metselaar (19) on the other, have already performed conductivity measurements on samples formulated as $3Bi_2O_3$–$2MoO_3$ or $Bi_6Mo_2O_{15}$. In both studies the ionic transference number of the oxide anion was determined to be ≅1 by measuring the emf of an oxygen gas concentration cell. From our determination, $3Bi_2O_3$–$2MoO_3$ or $Bi_{30}Mo_{10}O_{75}$ is a two phase mixture, containing a major amount of the upper limit of the $Bi_xMo_{10}O_\delta$-type solid solution (with $x = 27.75$), combined with some $Bi_{38}Mo_7O_{78}$. Thereby the $Bi_xMo_{10}O_\delta$-type solid solution (as $3Bi_2O_3$–$2MoO_3$) should exhibit interesting oxide anionic conduction properties. To confirm this assumption, impedance spectroscopy measurements were carried out on $Bi_{26}Mo_{10}O_\delta$, $Bi_{27.5}Mo_{10}O_\delta$, and $Bi_{30}Mo_{10}O_\delta$ (or $3Bi_2O_3$–$2MoO_3$) compounds, as well as $Bi_{26}Mo_8V_2O_\delta$ and $Bi_{26}Mo_7V_3O_\delta$ ones. Arrhenius plots were deduced and are reported on Fig. 11. With $3Bi_2O_3$–$2MoO_3$, within the temperature range studied, our plot is in very good agreement with those reported by the above mentioned authors (18, 19). The activation energy associated with the Arrhenius straight line is 0.56 eV, similar to those reported by Takahashi and Boon: 0.60 and 0.55 eV, respectively.

The Arrhenius plot dealing with $Bi_{27.5}Mo_{10}O_\delta$, the upper limit of the solid solution, is roughly parallel to that of $3Bi_2O_3$–$2MoO_3$, but its conductivity is slightly higher as expected with a single phase compound. We can also notice a small slope change at about 350°C, with $E_a \cong 0.46$ and 0.67 eV, above and below this temperature, respectively. This could be correlated with a smooth phase transition of the disorder–order type, as usually observed in γ-type BIMEVOX (20), but further experiments are needed to explain this behavior.

Regarding $Bi_{26}Mo_{10}O_\delta$, a clear slope change is observed at a temperature close to 300°C. This change is likely correlated with the triclinic–monoclinic reversible phase transition already observed by HTXRD and DSC. The high-temperature domain, probably corresponding to the monoclinic polymorph, exhibits an activation energy $E_a \cong 0.47$ eV similar to that of $Bi_{27.5}Mo_{10}O_\delta$, while the low-temperature domain is associated with a higher $E_a = 1.05$ eV.

The effect of Mo/V substitution is clearly observed on the compounds corresponding to the same Bi/(Mo + V) ratio = 26/10. The conductivity markedly decreases with increasing V content while the activation energy increases. For instance when $10^3/T = 1.7$, the conductivity of $Bi_{26}Mo_7V_3O_\delta$ ($E_a \cong 1$ eV) is about three orders of magnitude lower than that of $Bi_{26}Mo_{10}O_\delta$ ($E_a \cong 0.46$ eV).

CONCLUSION

The O atoms of the $[Bi_{12}O_{14}]_\infty$ columns, strongly bounded to the Bi atoms, are likely not involved in the oxygen anionic diffusion process in this family of materials. A more plausible hypothesis can be tentatively suggested to account for the conductivity: it could result from an eventual interstitial O atom or O vacancy, according to the stoichiometric problems of O content encountered during the crystal structure determinations of these compounds. This problem of stoichiometry seems to be localized in the MoO_4 (or Mo, VO_4) units where, unlike in the $[Bi_{12}O_{14}]_\infty$ columns, the atomic displacements of the atoms display unusual high values correlated with some softness

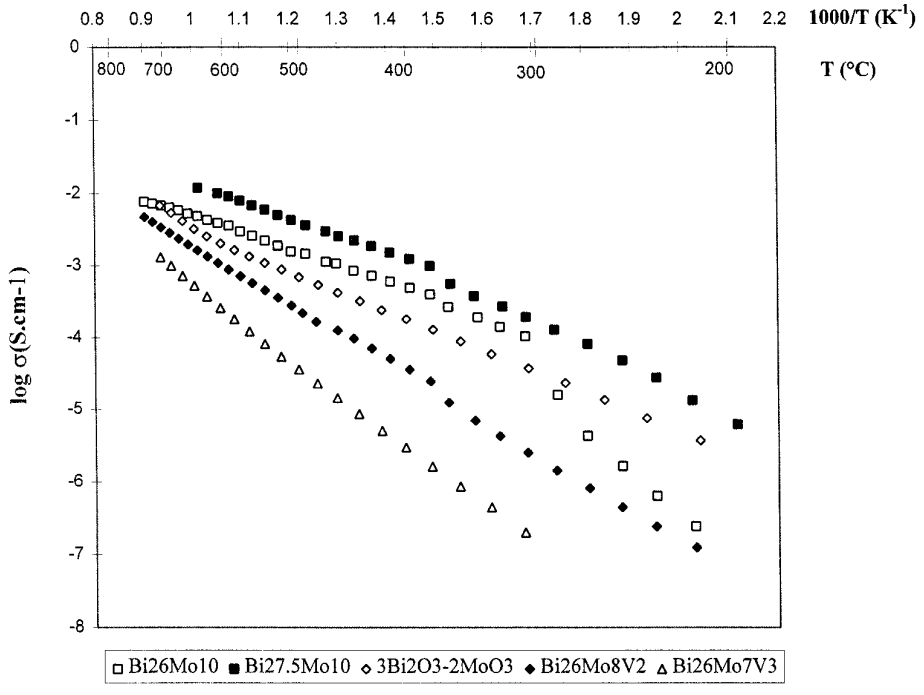

FIG. 11. Arrhenius plots corresponding to $Bi_{26}Mo_{10}O_{\delta}$, $Bi_{27.5}Mo_{10}O_{\delta}$, $3Bi_2O_3$–$2MoO_3$, $Bi_{26}Mo_8V_2O_{\delta}$, and $Bi_{26}Mo_7V_3O_{\delta}$.

of this part of the lattice which could favor the O anion mobility. This assumption would be in agreement with the striking similitude between this part of the structures and the scheelite-type compounds which exhibit oxide anionic conductivity too in $PbMoO_4$ and $PbWO_4$ (21), or mixed ionic-electronic conductivity in $BiVO_4$ and doped derivatives (22). Indeed, in both families, the heavy cation Bi^{3+} or Pb^{2+} is characterized by an eightfold oxygen coordination, while the lighter Mo^{6+}, W^{6+}, and V^{5+} are tetrahedrally coordinated. This common structural arrangement likely induces the common oxide anion conduction property.

Further experiments are in progress to understand the correlation between the structural parameters and the electrical properties of this solid solution.

REFERENCES

1. R. N. Vannier, G. Mairesse, F. Abraham, and G. Nowogrocki, *J. Solid State Chem.* **103,** 441 (1993).
2. D. J. Buttrey, T. Vogt, U. Wildgruber, and W. R. Robinson, *J. Solid State Chem.* **111,** 118 (1994).
3. R. K. Grasselli and J. F. Burrington, *Adv. Catal.* **30,** 133 (1981).
4. R. K. Grasselli, *J. Chem. Educ.* **63,** 216 (1986).
5. R. Kohlmuller and J. P. Badaud, *Bull. Soc. Chi. Fr.* **10,** 3434 (1969).
6. L. Ya. Erman, E. L. Galperin, and B. P. Soboler, *Russ. J. Inorg. Chem.* (*Engl. Transl.*) **16,** 258 (1971).
7. T. U. Chen and G. S. Smith, *J. Solid State Chem.* **13,** 288 (1975).
8. M. Egashira, K. Matsuo, S. Kagawa, and T. Seiyama, *J. Catal.* **58,** 409 (1979).
9. D. J. Buttrey, D. A. Jefferson, and J. M. Thomas, *Philos. Mag. A* **53(6),** 897 (1986).
10. D. J. Buttrey, D. A. Jefferson, and J. M. Thomas, *Mater. Res. Bull.* **21,** 739 (1986).
11. S. Miyazawa, A. Kawana, H. Koizumi, and H. Iwasaki, *Mater. Res. Bull.* **9,** 41 (1974).
12. J. De Meulenaer and H. Tompa, *Acta Crystallogr.* **19,** 1014 (1965).
13. D. T. Cromer and D. Liberman, *J. Chem. Phys.* **53,** 1891 (1970).
14. S. Seong, K. A. Yee, and T. A. Albright, *J. Am. Chem. Soc.* **115,** 1981 (1993).
15. F. Abraham and O. Mentre, *J. Solid State Chem.* **109,** 127 (1994).
16. I. D. Brown and R. D. Shannon, *Acta Crystallogr. Sect. A* **29,** 266 (1973).
17. I. D. Brown and D. Altermatt, *Acta Crystallogr. Sect. B* **41,** 244 (1985).
18. T. Takahashi, T. Esaka, and H. Iwahawa, *J. Appl. Electrochem.* **7,** 31 (1977).
19. L. Boon and R. Metselaar, *Solid State Ionics* **16,** 201 (1985).
20. E. Pernot, M. Anne, M. Bacmann, P. Strobel, J. Fouletier, R. N. Vannier, G. Mairesse, F. Abraham, and G. Nowogrocki, *Solid State Ionics* **70/71,** 259 (1994).
21. J. A. Groenink and H. Binsma, *J. Solid State Chem.* **29,** 227 (1979).
22. L. Hoffart, U. Heider, L. Jorissen, R. A. Huggins, and W. Witschel, *Solid State Ionics* **72,** 195 (1994).